

Structure and Dynamics of a Molecular Hydrogel Derived from a Tripodal Chalamide

Samrat Mukhopadhyay,[†] Uday Maitra,^{*†} Ira,[‡] Guruswamy Krishnamoorthy,[‡] Judith Schmidt,[¶] and Yeshayahu Talmon[¶]

Contribution from the Department of Organic Chemistry, Indian Institute of Science, Bangalore 560 012 India, Department of Chemical Sciences, Tata Institute of Fundamental Research, Mumbai 400 005, India, and Department of Chemical Engineering, Technion-Israel Institute of Technology, Haifa 32000, Israel

Received June 1, 2004; E-mail: maitra@orgchem.iisc.ernet.in

Abstract: Tripodal chalamide **1** is a supergelator of aqueous fluids. A variety of physical techniques, including cryo-transmission electron microscopy (TEM), circular dichroism (CD), steady-state fluorescence, time-resolved fluorescence, and dynamic light-scattering, were employed to understand the structure and dynamics of the gel. Fluorescent probes [ANS (8-anilino-1-naphthalene-sulfonic acid) and pyrene] reported two critical aggregation concentrations (CAC₁ and CAC₂) of **1** in predominantly aqueous media, with the minimum gel concentration (MGC) being close to CAC₂. Fluorescence lifetime measurements with pyrene revealed ineffective quenching of pyrene fluorescence by oxygen, possibly caused by slower Brownian diffusion due to the enhanced viscosity in the gel phase. The study of the gelation kinetics by monitoring the ultrafast dynamics of ANS revealed a progressive increase in the aggregate size and the microviscosity of the aqueous pool encompassed by the self-assembled fibrillar network (SAFIN) during the gelation. The striking difference between microviscosity and bulk (macroscopic) viscosity of the gel is also discussed.

1. Introduction

The formation of gels in water has been well documented with polymers and biopolymers.¹ Such materials are known as *hydrogels* or *aqueous gels*. Gelation with this class of molecules is believed to occur by chemical and/or physical cross-linking of polymeric chains, leading to the formation of a highly intertwined three-dimensional network, which restrains water molecules by surface tensional forces. When the driving forces for gelation involve molecular self-assembly through noncovalent physical forces, the resulting hydrogels are termed as physical gels or *molecular gels*.² The past decade has witnessed a rapid growth in this area of nonpolymeric gels. Compared to organogels,³ reports on molecular hydrogels have been scarce but have been rapidly increasing in recent years.⁴ A wide variety of molecular species involving amino acid derivatives,⁵ polypep-

tides,⁶ carbohydrate derivatives,⁷ gemini surfactants/bolamphiphiles,⁸ bile acids,⁹ and others¹⁰ have been shown to act as gelators of aqueous fluids. These hydrogels are of great

[†] Indian Institute of Science.

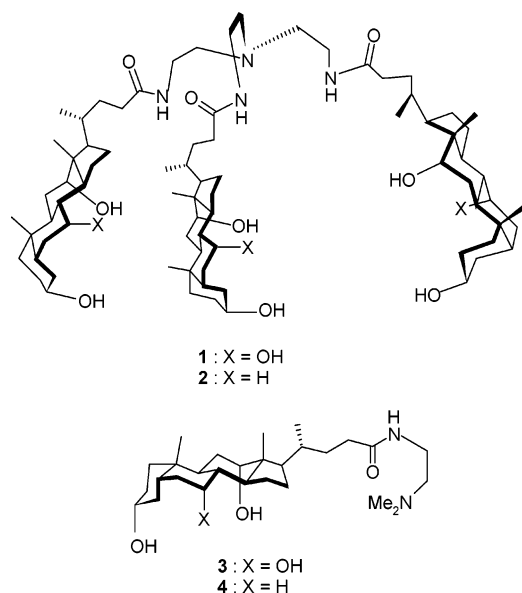
[‡] Tata Institute of Fundamental Research.

[¶] Technion-Israel Institute of Technology.

- (1) (a) Terech, P. *Encyclopedia of Surface and Colloid Science*; Marcel Dekker: New York, 2002; pp 2299–2319. (b) Guenet J. M. *Thermoreversible Gelation of Polymers and Biopolymers*; Academic Press: New York, 1992.
- (2) *Molecular Gels*; Terech, P., Wiess, R. G., Eds.; Kluwer Academic Publishers: The Netherlands, 2004.
- (3) For recent reviews on organogels, see: (a) Terech, P.; Wiess, R. G. *Chem. Rev.* **1997**, *97*, 3133. (b) van Esch, J. H.; Feringa, B. L. *Angew. Chem., Int. Ed.* **2000**, *39*, 2263. (c) Abdallah, D. J.; Weiss, R. G. *Adv. Mater.* **2000**, *12*, 1237. (d) See ref 2.
- (4) (a) Bhattacharya, S.; Maitra, U.; Mukhopadhyay, S.; Srivastava, A. In *Molecular Gels*; Terech, P., Wiess, R. G., Eds.; Kluwer Academic Publishers: The Netherlands, 2004. (b) Estroff, L. A.; Hamilton, A. D. *Chem. Rev.* **2004**, *104*, 1201.

- (5) (a) Imae, T.; Takahashi, Y.; Muramatsu, H. *J. Am. Chem. Soc.* **1992**, *114*, 3414. (b) Fuhrhop, J.-H.; Spiroski, D.; Boettcher, C. *J. Am. Chem. Soc.* **1993**, *115*, 1600. (c) Menger, F. M.; Caran, K. L. *J. Am. Chem. Soc.* **2000**, *122*, 11679. (d) Estroff, L. A.; Hamilton, A. D. *Angew. Chem., Int. Ed.* **2000**, *39*, 3447. (e) Frkanec, L.; Jokic, M.; Makarevic, J.; Wolsperger, K.; Zinic, M. *J. Am. Chem. Soc.* **2002**, *124*, 9716. (f) Suzuki, M.; Yumoto, M.; Kimura, M.; Shirai, H.; Hanabusa, K. *Chem. Commun.* **2002**, 884. (g) Heeres, A.; van der Pol, C.; Stuart, M.; Friggeri, A.; Feringa, B. L.; van Esch, J. *J. Am. Chem. Soc.* **2003**, *125*, 14252. (h) Suzuki, M.; Yumoto, M.; Kimura, M.; Shirai, H.; Hanabusa, K. *Chem.—Eur. J.* **2003**, *9*, 348. (i) van Bommel, K. J. C.; van der Pol, C.; Muizebelt, I.; Friggeri, A.; Heeres, A.; Meetsma, A.; Feringa, B. L.; van Esch, J. *Angew. Chem., Int. Ed.* **2004**, *43*, 1663.
- (6) (a) Hartgerink, J. D.; Beniash, E.; Stupp, S. I. *Proc. Natl. Acad. Sci. U.S.A.* **2002**, *99*, 5133. (b) Aggeli, A.; Bell, M.; Boden, N.; Keen, J. N.; Knowles, P. F.; McLeish, T. C. B.; Pitkeathly, M.; Radford, S. E. *Nature* **1997**, *386*, 259. (c) Collier, J. H.; Hu, B.-H.; Ruberti, J. W.; Zhang, J.; Shum, P.; Thompson, D. H.; Messersmith, P. B. *J. Am. Chem. Soc.* **2001**, *123*, 9463. (d) Xing, B.; Yu, C.-W.; Chow, K.-H.; Ho, P.-L.; Fu, D.; Xu, B. *J. Am. Chem. Soc.* **2002**, *124*, 14846. (e) Schneider, J. P.; Pochan, D. J.; Ozbas, B.; Rajagopal, K.; Pakstis, L.; Kretsinger, J. *J. Am. Chem. Soc.* **2002**, *124*, 15030. (f) Pochan, D. J.; Schneider, J. P.; Kretsinger, J.; Ozbas, B.; Rajagopal, K.; Haines, L. *J. Am. Chem. Soc.* **2003**, *125*, 11802. (g) Claussen, R. C.; Rabatic, B. M.; Stupp, S. I. *J. Am. Chem. Soc.* **2003**, *125*, 12680.
- (7) (a) Pffannemuller, B.; Welte, W. *Chem. Phys. Lipids* **1985**, *37*, 227. (b) Furhorp, J.-H.; Schnieder, P.; Rosenberg, J.; Boekema, E. *J. Am. Chem. Soc.* **1987**, *109*, 3387. (c) Bhattacharya, S.; Acharya, S. N. *G. Chem. Mater.* **1999**, *11*, 3504. (d) Kobayashi, H.; Friggeri, A.; Koumoto, K.; Amaike, M.; Shinkai, S.; Reinhoudt, D. N. *Org. Lett.* **2002**, *4*, 1423. (e) Jung, J. H.; Shinkai, S.; Shimizu, T. *Chem.—Eur. J.* **2002**, *8*, 2684. (f) Kiyonaka, S.; Shinkai, S.; Hamachi, I. *Chem.—Eur. J.* **2003**, *9*, 976.
- (8) (a) Newkome, G. R.; Baker, G. R.; Arai, S.; Saunders, M. J.; Russo, P. S.; Theriot, K. J.; Moorefield, C. N.; Rogers, L. E.; Miller, J. E.; Lieux, T. R.; Murray, M. E.; Phillips, B.; Pascal, L. *J. Am. Chem. Soc.* **1990**, *112*, 8458. (b) Oda, R.; Huc, I.; Candau, S. *J. Angew. Chem., Int. Ed.* **1998**, *37*, 2689. (c) Iwaura, R.; Yoshida, K.; Masuda, M.; Yase, K.; Shimizu, T. *Chem. Mater.* **2002**, *14*, 3047. (d) Menger, F. M.; Peresypkin, A. *J. Am. Chem. Soc.* **2003**, *125*, 5340.

Chart 1



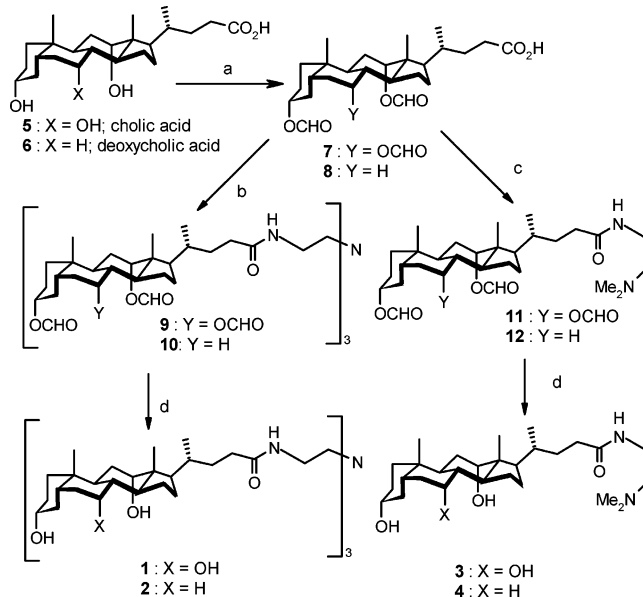
importance due to the fact that they are potential materials for biomedical applications, such as drug-delivery systems, tissue engineering, semi-wet biomaterials for protein microarray, and so forth.¹¹ Recently, the advantages of using the molecular hydrogels over traditional polymeric hydrogels have been reviewed.¹² In addition to potential applications, gels are materials with intriguing features owing to the coexistence of solid (the networked fibrous structure) and liquid (entrapped solvent molecules) phases. These gels are viscoelastic materials since they display properties of both solids (elasticity) and liquids (viscosity).¹³ Structural analysis of these materials is not straightforward since they do not lend themselves to studies at atomic resolutions. Applications of a variety of physical techniques are required to gain insights into the complex nature of the gel phase.^{2–4}

We have recently described the efficient gelation ability of a novel tripodal cholamide in aqueous media.¹⁴ The gel formation was associated with the formation of hydrophobic pockets in a predominantly aqueous medium. The rotational dynamics of polarity-sensitive organic dyes partitioned in the hydrophobic region and in the aqueous phase of the gel was determined using the picosecond time-resolved fluorescence method.¹⁵ The ap-

plication of such hydrogels in the template-directed preparation of nanotubes of inorganic oxides and sulfates has also been reported.¹⁶ Herein, we disclose the synthetic protocols and detailed studies on the aggregation behavior of tripodal cholamide **1**, deoxycholamide **2**, and their monomeric analogues, **3** and **4** (Chart 1). A combination of microscopic and spectroscopic techniques was used to understand the structure and dynamics of gels. Also, we provide insights into the time course of the gelation process using a *double-kinetic* experiment.

2. Results

2.1. Synthesis. The tripodal bile acid derivatives (nonahydroxy **1** and hexahydroxy **2**) were prepared in three steps from cholic and deoxycholic acid, respectively (Scheme 1). Formyl-

Scheme 1^a

^a (a) HCO₂H, rt, 5 h. (b) DCC–DMAP/N[CH₂CH₂NH₂]₃ in DCM, 12 h. (c) DCC–DMAP/Me₂NCH₂CH₂NH₂ in DCM, 5 h. (d) With 5% KOH–MeOH.

protected bile acids were coupled with tren to obtain the tripodal architecture. In the next step, the formyl groups were cleaved to obtain the free hydroxy tripodal bile acid derivatives. *N,N*-Dimethylethylenediamine was used to obtain monomeric analogues.

2.2. Behavior in Aqueous Media. Nonahydroxy **1** and hexahydroxy **2** were insoluble in water. The protonated salts, such as **1**·HCl and **2**·HCl, have limited solubility in water. However, upon the addition of a small amount (5–20%) of organic cosolvents (e.g., EtOH, MeOH, CH₃CN, DMSO, DMF, and acetone), clear solutions were obtained. Compound **1** formed a transparent gel (Figure 1A) from such solutions in a few minutes, but **2** failed to form a gel under all of the conditions we studied. Monomeric analogues (**3** and **4**) also did not act as gelators of aqueous fluids. They formed either precipitates or clear solutions depending on the concentration of the compound and the composition of the cosolvents. The “best” gels (transparent and thermally stable) were obtained in acetic acid–

- (9) (a) Schryver, S. B. *R. Soc. Proc., Ser. B* **1914**, 87, 366. (b) Schryver, S. B. *R. Soc. Proc., Ser. B* **1916**, 89, 361. (c) Sobotka, H.; Czeczowiczka, N. *J. Colloid Sci.* **1958**, 13, 188. (d) Rich, A.; Blow, D. M. *Nature* **1958**, 182, 423. (e) Blow, D. M.; Rich, A. *J. Am. Chem. Soc.* **1960**, 82, 3566. (f) Igimi, H.; Carey, M. *J. Lipid Res.* **1980**, 21, 72. (g) Terech, P.; Smith, W. G.; Weiss, R. G. *J. Chem. Soc., Faraday Trans.* **1996**, 92, 3157. (h) Jover, A.; Mejjide, F.; Núñez, E. R.; Tato, J. V. *Langmuir* **1996**, 12, 1789. (i) Lopez, F.; Samseth, J.; Mortensen, K.; Rosenqvist, E.; Rouch, J. *Langmuir* **1996**, 12, 6188.
- (10) (a) Fuhrhop, J.-H.; Demoulin, C.; Rosenberg, J.; Boettcher, C. *J. Am. Chem. Soc.* **1990**, 112, 2827. (b) Haines, S. R.; Harrison, R. G. *Chem. Commun.* **2002**, 2846. (c) Marmillon, C.; Gaufré, F.; Gulik-Krzywicki, T.; Loup, C.; Caminade, A.-M.; Majoral, J.-P.; Vors, J.-P.; Rump, E. *Angew. Chem., Int. Ed.* **2001**, 40, 2626. (d) Park, S. M.; Lee, Y. S.; Kim, B. H. *Chem. Commun.* **2003**, 2912.
- (11) (a) Lee, K. Y.; Moony, D. J. *Chem. Rev.* **2001**, 101, 1869. (b) Miyata, T.; Uragami, T.; Nakamae, K. *Adv. Drug Delivery Rev.* **2002**, 54, 79. (c) Kiyonaka, S.; Sada, K.; Yoshimura, I.; Shinkai, S.; Kato, N.; Hamachi, I. *Nat. Mater.* **2004**, 3, 58.
- (12) Tiller, J. C. *Angew. Chem., Int. Ed.* **2003**, 42, 3072.
- (13) Ross-Murphy, S. B. *Physical Techniques for the Study of Food Biopolymers*; Blackie: London, 1994.
- (14) Maitra, U.; Mukhopadhyay, S.; Sarkar, A.; Rao, P.; Indi, S. S. *Angew. Chem., Int. Ed.* **2001**, 40, 2281.

- (15) Mukhopadhyay, S.; Ira, Krishnamoorthy, G.; Maitra, U. *J. Phys. Chem. B.* **2003**, 107, 2189.
- (16) Gundiah, G.; Mukhopadhyay, S.; Tumkurkar, U. G.; Govindaraj, A.; Maitra, U.; Rao, C. N. R. *J. Mater. Chem.* **2003**, 13, 2118.

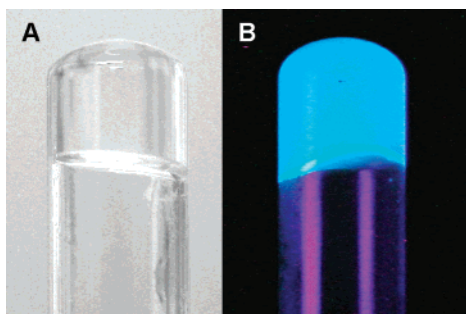


Figure 1. (A) Transparent gel: $[1] = 9$ mM in 20% AcOH–H₂O. (B) Luminescent gel: $[1] = 5$ mM and $[ANS] = 30$ μ M.

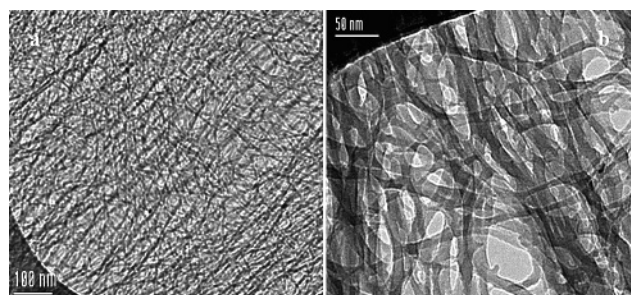


Figure 2. Cryo-TEM images of the gel (0.75 mM) in 20% AcOH–water at two different magnifications. Bars represent 100 nm (a) and 50 nm (b).

Table 1. Minimum Gel Concentrations (MGC) of **1** as a Function of Solvent Composition at Room Temperature

solvent composition (v/v)	MGC (mM)
20% AcOH–water	0.75
1% AcOH–water	0.60
0.05% AcOH–water	0.30
0.01% AcOH–water	0.15

water systems ranging from 0.01 to 30% AcOH in water, depending on the gelator concentration (Table 1). These gels were thermoreversible and thixotropic in nature, and they were stable for more than 3 years when kept in sealed tubes. Gels were formed under remarkably low concentrations of the gelator. The minimum gel concentration was as low as 0.15 mM,¹⁷ implying the immobilization (apparent rigidification) of more than 3×10^5 water molecules by one molecule of **1**. To the best of our knowledge, among the hydrogelators known to date, **1** forms gels at the lowest gelator concentration.

2.3. Electron Microscopy. Cryogenic temperature transmission electron microscopy (cryo-TEM) images of vitrified specimens of the gel formed in a solution of 0.75 mM **1** in 20% AcOH–water are shown in Figure 2. At the two magnifications shown, the gel appears as a well-developed intertwined network. The higher magnification view of Figure 2b reveals that the network is made of very thin, flat ribbons (2–5 nm wide). That those are indeed flat ribbons can be deduced from the uniformity of optical density across each one of them. One should realize that in the TEM, all structures in the thin specimen, approximately 100 nm thick, are projected and seen clearly in the image. This gives the impression of the presence of much more polymer in the gel than its actual concentration.

2.4. Circular Dichroism. To investigate the chiral structure of gels, CD experiments were performed on the gel derived

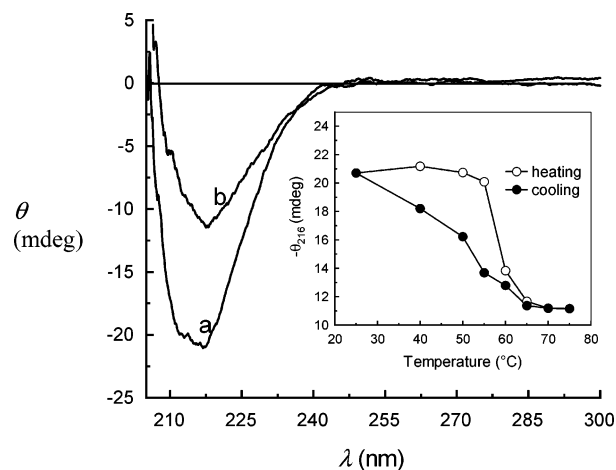


Figure 3. CD spectra of the gel at 25 °C (a) and of the sol at 75 °C (b) from **1**·HCl (3.0 mM in 20% EtOH–water). The inset shows the variable temperature CD of the gel (heating and cooling cycle).

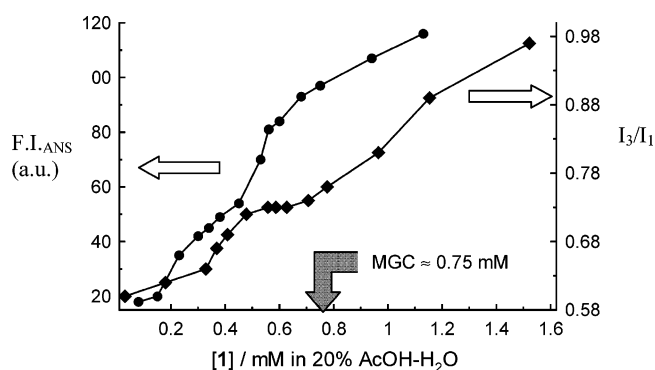


Figure 4. Change in the fluorescence intensity of ANS (10 μ M) and the I_3/I_1 ratio (pyrene fluorescence, $[pyrene] = 0.5$ μ M) as a function of the gelator concentration at 25 °C.

from the hydrochloride salt ($[1\cdot HCl] = 3$ mM in 20% EtOH–water). A negative CD band (amide chromophore) was observed for both isotropic solution ($[1\cdot HCl] = 3$ mM in neat EtOH) and gel. The CD band intensity at 216 nm was twice as much (21 mdeg) for gel than the intensity for the isotropic solution of **1**·HCl in neat EtOH (10 mdeg), which does not form a gel (not shown). Figure 3 shows that the intensity of the CD band diminishes to about 11 mdeg at the gel melting temperature ($T_{gel} \approx 55$ °C). The variable temperature CD showed hysteresis (nonidentical heating and cooling curves).

2.5. Steady-State Fluorescence of Pyrene. Pyrene was used as an external fluorescent probe to determine the critical aggregation concentration. The vibronic fine structure of the pyrene fluorescence is indicative of local polarity of the binding site. The plot (Figure 4) of the ratio of two vibronic bands (I_3/I_1) versus the gelator concentration (in 20% AcOH–water) suggested two critical aggregation concentration (CAC) ranges ($CAC_1 \approx 0.4$ mM and $CAC_2 \approx 0.8$ mM). The gelation was visually observed at 0.75 mM. No excimer formation was observed in the gel phase. With lower amounts of AcOH (e.g., 1% AcOH–water), the minimum gel concentration was lower (0.6 mM) and I_3/I_1 values were higher (Table 2). Another interesting observation was the formation of an excimer band (centered on 480 nm) in the pyrene fluorescence spectrum for (micellar) aggregates of **1** in 1% AcOH–water below a minimum gel concentration (i.e., below 0.6 mM). In the gel

(17) Partial gelations could still be observed at micromolar concentrations (75 μ M) of **1**, but these gels were unstable at room temperature.

Table 2. Fluorescence Lifetimes and I_3/I_1 Values for Pyrene in Solutions, in Aggregates, and in Gels at 25 °C

sample ([pyrene] \approx 0.5 μ M)	τ (ns) ^a	I_3/I_1 ^b
water	135	0.58
20% AcOH–water	137	0.61
aggregate of 1 (0.6 mM) in 20% AcOH–water	170	0.75
gel from 1 (5.3 mM) in 20% AcOH–water	226	1.10
aggregate of 1 (42 μ M) in 1% AcOH–water	239 (68) ^c	1.42
gel from 1 (0.8 mM) in 1% AcOH–water	324	1.53

^a Errors are $< \pm 5$ ns. ^b Errors are $< \pm 0.05$. ^c Excimer lifetime.

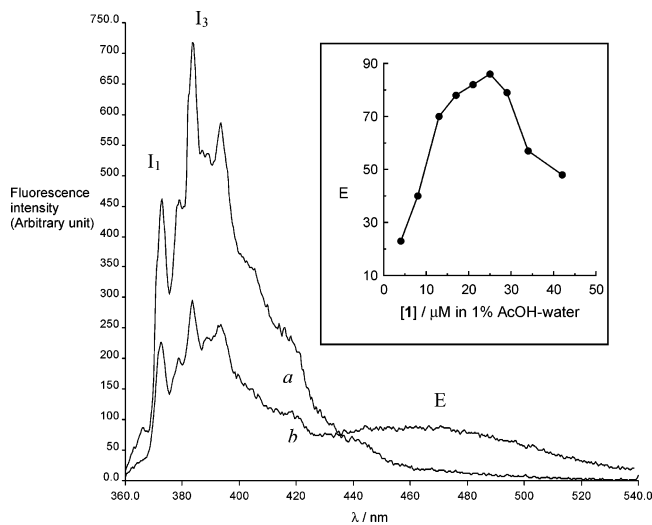


Figure 5. Fluorescence spectra of pyrene in (a) gel ([**1**] = 1.7 mM) and (b) micellar aggregate ([**1**] = 25 μ M) in 1% AcOH–water. I_1 , I_3 , and E are the first vibronic band, the third vibronic band, and the excimer band, respectively. The inset shows the variation of the excimer intensity (E at 475 nm) as a function of [**1**] below MGC.

phase (i.e., at a higher concentration of **1**), this band disappeared (Figure 5).

2.6. Steady-State Fluorescence of ANS. Using steady-state fluorescence titration, we have studied the interaction of ANS (8-anilino-1-naphthalene sulfonic acid) with increasing amounts of **1** to monitor the onset of the aggregation process. The plot (Figure 4) of the intensity of ANS fluorescence versus gelator concentration (in 20% AcOH–water) also suggested two critical aggregation concentration ranges (~ 0.3 and ~ 0.7 mM). Steady-state fluorescence anisotropy of ANS in gel decreases as a function of temperature and remains almost constant beyond the gel melting temperature. This indicates higher mobility of ANS in the sol phase compared to that in the gel phase. The variable temperature anisotropy (Figure 6) exhibits hysteresis in the sol-to-gel phase transition, as observed in the variable temperature CD.

2.7. Time-Resolved Fluorescence. Fluorescence lifetime (τ) of pyrene in nondeoxygenated water was found to be ~ 135 ns. In the presence of increasing amounts (1–20% v/v) of acetic acid in water, change in the fluorescence lifetime (τ) of pyrene was insignificant (135–137 ns). However, τ increased in the aggregates and gels derived from **1** in 20% AcOH–water (Table 2). In 1% AcOH–water, even longer fluorescence lifetimes were observed for pyrene (239 and 324 ns in the micellar aggregate

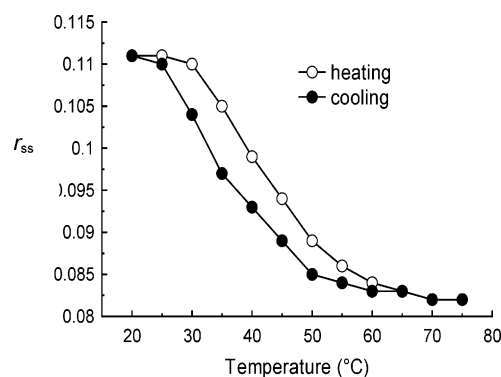


Figure 6. Temperature dependence of the steady-state fluorescence anisotropy (r_{ss}) of ANS in the gel from nonhydroxy salt (3.0 mM **1**·HCl) in 20% EtOH–water.

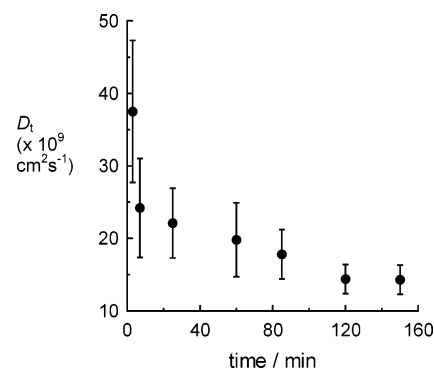


Figure 7. Change in the average translational diffusion coefficient (D_t) of the aggregates as a function of time during the gelation at 25 °C. [**1**] = 5.3 mM. Bars represent the measured polydispersity.

and in the gel, respectively), which are close to those observed in deoxygenated media (~ 400 ns), indicating ineffective quenching by oxygen. Excimer lifetime was found to be ~ 68 ns in the micellar aggregate of **1** in 1% AcOH–water.

2.8. Dynamic Light-Scattering. The average translational diffusion coefficient (D_t) of the aggregates is inversely proportional to the aggregate size and the viscosity by the Stokes–Einstein equation for translational diffusion (eq 1).

$$D_t = \frac{kT}{6\pi\eta R_h} \quad (1)$$

where η is the solvent viscosity, and R_h is the mean hydrodynamic radius of the diffusing unit.

For micellar aggregates (0.6 mM **1** in 20% AcOH–water), D_t was about $70 \times 10^{-9} \text{ cm}^2 \text{ s}^{-1}$. The micellization was fast and did not show any change in D_t with time. On the contrary, the gelation (5.3 mM **1** in 20% AcOH–water) process was slower and could be monitored by the dynamic light-scattering technique. D_t was found to decrease (from 38×10^{-9} to $14 \times 10^{-9} \text{ cm}^2 \text{ s}^{-1}$) as a function of time during the gelation process (Figure 7). No significant change was observed after 2 h. Also, the polydispersity, which is related to the heterogeneity in the aggregate structure in terms of the aggregation number, was found to decrease as a function of time during gelation. The data clearly show the progressive increase in the homogeneity of the aggregate structure during the course of gelation.

2.9. Time-Resolved Fluorescence Anisotropy of ANS during Gelation. The time-resolved decay of the fluorescence anisotropy [$r(t)$] of ANS, in both water and 20% AcOH–water,

Table 3. Recovered Rotational Correlation Times of ANS (ϕ_b for bound and ϕ_f for free) from the Time-Resolved Anisotropy Experiments in Isotropic Solution, Premicellar Aggregate, Micellar Aggregate, and Gel from **1** under Equilibrium Conditions at 25 °C^a

sample	[1] (mM)	ϕ_b (ns)	ϕ_f (ns)
20% AcOH–H ₂ O below CAC ₁ of 1 in 20% AcOH–H ₂ O	0.2	2.1	0.1
above CAC ₁ and below CAC ₂	0.6	4.9	0.2
above CAC ₂ and above MGC	5.3	12.1	1.0

^a Errors in the analysis were <10%.

yielded a single-exponential decay with a rotational correlation time of about 0.1 ns. The molecular volume of ANS was calculated (*ab initio*) and found to be 282.9 Å³. The calculated rotational correlation time of ANS in 20% AcOH–water (viscosity = 1.2 cP at 25 °C) was found to be 84 ps, obtained by the Stokes–Einstein equation for rotational diffusion (eq 2), which is close to the experimentally determined value, 90 ± 10 ps (~0.1 ns). When data were collected for compound **1**, dissolved in 20% AcOH–water, $[r(t)]$ of ANS was more complex and could be satisfactorily explained by a bi-exponential decay function. Since this behavior could be indicative of two populations of the fluorescent probe, $[r(t)]$ was analyzed by a two-population model (see section 5.8 for the method). The intensity decay analysis (fluorescence lifetimes) also suggested the presence of two populations; thus, the two recovered rotational correlation time data could be assigned to free (exposed to aqueous phase) and bound (to hydrophobic pockets) forms of ANS. This is also justified by the short and long values of the rotational correlation times. Similar data were recovered when the anisotropy decay curves were analyzed by a single-population model (as a sum of two exponentials).

At a concentration of 0.2 mM **1** (below the first critical aggregation concentration, CAC₁), ANS has a longer rotational correlation time of 2.1 ns, which increased to 4.9 ns with the increase in the concentration of **1** to 0.6 mM (above CAC₁). The shorter component (≤0.2 ns for the aqueous population of ANS) did not show a significant change (Table 3). Further increase in the gelator concentration to 5.3 mM (well above MGC) significantly changed the dynamics of both bound (12.1 ns) and free (1.0 ns) ANS. Therefore, we undertook the “double-kinetic” experiments (fluorescence anisotropy decay kinetics as a function of gelation kinetics) as follows. Compound **1** was dissolved in AcOH; an appropriate amount of water was added, and the time evolutions of both ϕ_b and ϕ_f were determined (Table 4). The investigation on the gelation kinetics using time-dependent anisotropy (a double-kinetics approach)²⁵ indicated a gradual change in both the rotational correlation times (ϕ_b for “bound” ANS and ϕ_f for “free” ANS). The change in the microviscosity of the aqueous phase (from ~3 to 13 cP) during

Table 4. Change in the Rotational Correlation Times of ANS as a Function of Time during the Gelation (at 25 °C) Obtained from the Double-Kinetics Experiments

time after mixing (min)	Rotational Correlation Times ^a		
	ϕ_b (ns)	ϕ_f (ns)	η_{aq}^b (cP)
4	3.7	0.2	2.7
10	3.9	0.4	5.3
23	4.8	0.6	8.0
55	7.4	0.7	9.3
126	11.0	1.0	13.3
160	12.1	1.0	13.3

^a Errors in the analysis are <±1.0 ns (for ϕ_b) and <±0.1 ns (for ϕ_f).
^b η_{aq} is the microviscosity felt by ANS.

the gelation process was estimated from the Stokes–Einstein equation for rotational diffusion (eq 2) using the rotational correlation time of the free probe (ϕ_f).

$$\phi = \frac{\eta V}{kT} \quad (2)$$

where V is the volume of the rotating unit, and η is the microviscosity experienced by ANS.

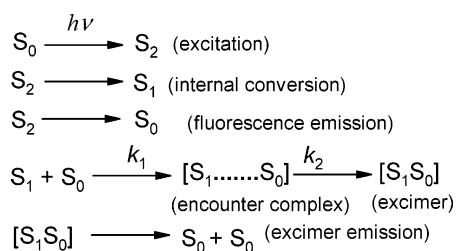
3. Discussion

3.1. Nanoscale Structure of Gel. Cryo-transmission electron microscopy was used to visualize the nanoscale structure of the gel. The advantages of using the cryo-TEM are 2-fold. The fast freezing of the samples upholds the hydrated morphology, and the staining agents are not required because of the intrinsic contrast between vitrified ice and the organic material.²⁹ A TEM image of the gel shows a network structure composed of entangled nanofibers (Figure 2) forming meshes, which are responsible for immobilizing the solvent molecules. These fibers are formed by one-dimensional growth of the supramolecular assembly of **1** in aqueous acids.

3.2. Amplification of Chirality in the Gel State. Circular dichroism spectra indicated that molecules are self-assembled in an asymmetric manner (e.g., helical) in the gel phase causing the amplification of the chirality in the gel phase, which can be attributed to the supramolecular chirality in the gel state. Around the melting temperature of the gel (~55 °C), the sharp decrease in the ellipticity indicates the loss of (supramolecular) chirality upon gel melting (Figure 3). The CD (at 216 nm) of the sol (11

- (18) (a) Kalyanasundaram, K. In *Photochemistry in Organized & Constrained Media*; Ramamurthy, V., Ed.; VCH Publishers: New York, 1991; Chapter 2. (b) Bohne, C.; Redmond, R. W.; Scaiano, J. C. In *Photochemistry in Organized & Constrained Media*; Ramamurthy, V., Ed.; VCH Publishers: New York, 1991; Chapter 3. (c) Kalyanasundaram, K.; Thomas, J. K. *J. Am. Chem. Soc.* **1977**, *99*, 2039. (d) Gouin, S.; Zhu, X. X. *Langmuir* **1998**, *14*, 4025.
- (19) Sahoo, L.; Sarangi, J.; Misra, P. K. *Bull. Chem. Soc. Jpn.* **2002**, *75*, 859.
- (20) Kweon, M.; Lee, Y. H.; Ahn, B. T.; Lee, M. *Bull. Korean Chem. Soc.* **1996**, *17*, 158.
- (21) (a) Nakajima, A. *Bull. Chem. Soc. Jpn.* **1973**, *46*, 2602. (b) Hara, K.; Ware, W. *Chem. Phys.* **1981**, *51*, 61. (c) Karpovich, D. S.; Blanchard, G. J. *J. Phys. Chem.* **1995**, *99*, 3951.
- (22) Slavik, J. *Biochim. Biophys. Acta* **1982**, *694*, 1.
- (23) Lakowicz, J. R. *Principles of Fluorescence Spectroscopy*; Plenum Press: New York, 1999.
- (24) (a) Maitra, U.; Kumar, P. V.; Chandra, N.; D'Souza, L. J.; Prasann, M. D.; Raju, A. R. *Chem. Commun.* **1999**, 595. (b) Maitra, U.; Kumar, P. V.; Sangeetha, N. M.; Babu, P.; Raju, A. R. *Tetrahedron: Asymmetry* **2001**, *12*, 477. (c) Babu, P.; Sangeetha, N. M.; Kumar, P. V.; Maitra, U.; Rissanen, K.; Raju, A. R. *Chem.—Eur. J.* **2003**, *9*, 1922.
- (25) (a) Saxena, A.; Udgaonkar, J. B.; Krishnamoorthy, G. In *Applications of Fluorescence Spectroscopy*; Hof, M., Ed.; Springer-Verlag: New York, 2004. (b) Krishnamoorthy, G. *Indian J. Biochem. Biophys.* **2003**, *40*, 147. (c) Maiti, N. C.; Krishna, M. M. G.; Britto, P. J.; Periasamy, N. *J. Phys. Chem. B* **1997**, *101*, 11051. (d) Lakshminikanth, G. S.; Krishnamoorthy, G. *Biophys. J.* **1999**, *77*, 1100.
- (26) Rotational relaxation time of ANS was estimated to be 161 ns (using the Perrin equation) in pure glycerol at 22.6 °C: Treloar, F. E. *Chem. Scr.* **1976**, *10*, 215.
- (27) Cortese, F.; Bauman, L. *J. Am. Chem. Soc.* **1935**, *57*, 1393.
- (28) Takahashi, A.; Sakai, M.; Kato, T. *Polym. J.* **1980**, *12*, 335.
- (29) (a) Talmon, Y. Cryogenic Temperature Transmission Electron Microscopy in the Study of Surfactant Systems. In *Modern Characterization Methods of Surfactant Systems*; Binks, B. P., Ed.; Marcel Dekker: New York, 1999; Chapter 5, pp 147–178. (b) Estroff, L. A.; Leiserowitz, L.; Addadi, L.; Weiner, S.; Hamilton, A. D. *Adv. Mater.* **2003**, *15*, 38.

Scheme 2



mdeg, which remains constant beyond T_{gel}) is close to that observed for an isotropic solution (~ 10 mdeg) of **1** in neat EtOH, suggesting nearly complete disruption of the aggregation.

3.3. Local Polarity and the Critical Aggregation Concentrations. The analysis of emission spectra from fluorescent probes has provided important details on the structure, dynamics, and transport in organized assemblies.¹⁸ A hydrophobic guest molecule, such as pyrene, is known to bind to the hydrophobic core of a micellar aggregate, including bile salt micelles.¹⁸ Fluorescence spectra of such fluorescent guest molecules carry information on the nature of the hydrophobic interior. The ratio of two vibronic bands (I_3/I_1) in the fluorescence spectrum of pyrene is indicative of the polarity (dielectric constant) of the binding site in the micelles/aggregates.^{18c} The critical aggregation concentrations (CACs) of **1** were determined from the dependence of I_3/I_1 on the gelator concentration from the equilibrium experiments. Two inflections (Figure 4) correspond to at least two steps of aggregation (primary and secondary aggregation). From the correlation of I_3/I_1 of pyrene and the $E_T(30)$ values reported by others, we infer that the hydrophobic interior of the gel phase has a dielectric constant similar to that of alcohols.¹⁹ With lower amounts of AcOH (e.g., 1% AcOH–water), the primary aggregation concentration ($\text{CAC}_1 \approx 25 \mu\text{M}$) was lower and I_3/I_1 values were higher (Table 2). Higher I_3/I_1 values indicate that the pyrene is in a more hydrophobic environment (away from the aqueous phase) in both aggregates and gels prepared in lower amounts of cosolvents in water. This is an example of a more pronounced hydrophobic effect of water when the concentration of organic cosolvent is lower. The absence of the excimer band for pyrene in the gel phase (i.e., at a higher concentration of **1**) could be explained as follows. The excimer formation dynamics is governed by two factors characterized by two rate constants: k_1 (viscosity dependent) and k_2 (solvent polarity dependent).²⁰ The first process (k_1) of bringing two pyrene (incorporated within the aggregates) closer to form an encounter complex is diffusion controlled and would be dependent on the solvent viscosity. If the viscosity is higher (e.g., in gels), the approach of two probe molecules (prerequisite to an excimer formation) gets hindered. The probability of the encounter complexes (loosely bound) being converted to the excimer (stronger complex) would be higher if the solvent polarity is high (1% AcOH–water > 20% AcOH–water) enough to necessitate the association of two hydrophobic probe molecules in the micellar aggregates (Scheme 2).

Pyrene has an unusually long fluorescence lifetime (~ 400 ns in deoxygenated cyclohexane) because the $S_1 \rightarrow S_0$ transition is partially forbidden.²¹ The fluorescence lifetime of pyrene (τ) is shortened in nondeoxygenated polar solvents of low viscosity because the two major rate processes depopulate the excited state; (i) nonradiative decay (k_{nr}) is more efficient in polar solvents, and (ii) freely diffusing oxygen (triplet) quenches

(bimolecular quenching rate constant, k_q) the long-lived S_1 (eq 3).

$$\tau = \frac{1}{k_r + k_{\text{nr}} + k_q[\text{O}_2]} \quad (3)$$

The time-resolved decay of the fluorescence intensity of pyrene provides more insights into the microenvironment of the aggregates. The fluorescence lifetime of pyrene (τ) increases when pyrene is solubilized in the micellar aggregate or in the gel phase (Table 2). This increase in τ is attributed to the decrease in both of the rate constants (k_{nr} and k_q). It is expected that quenching becomes inefficient since the diffusion coefficient of oxygen (D , which is inversely proportional to viscosity, η) is lowered due to the increase in the viscosity in the gel phase (eq 5). Our results indeed indicate that the pyrene is more effectively protected from the quenching by oxygen in the gel phase. Thus, in the gel phase, the major modification occurs in the quenching term ($k_q[\text{O}_2]$ component) of eq 3. The root-mean-square distance ($\sqrt{\Delta x^2}$) over which a quencher can diffuse during the excited-state lifetime (τ) is given by

$$\sqrt{\Delta x^2} = \sqrt{(2D\tau)} \quad (4)$$

$$k_q \propto D \propto 1/\eta \quad (5)$$

With lower amounts of acetic acid (1% v/v), due to the enhanced hydrophobic effect (compared to that of 20% AcOH–water), the aggregation is more pronounced (Table 1). Therefore, pyrene is even more effectively protected from quenching by $^3\text{O}_2$. A relatively nonpolar microenvironment around pyrene is also supported by a higher I_3/I_1 value (Table 2). In this case, the gelling condition seems to be more important than the gelator concentration. In the gel phase, the fluorescence lifetime of pyrene ($\tau \approx 324$ ns) approaches the value observed in *deoxygenated cyclohexane* (~ 400 ns).

A partially water-soluble fluorescent probe of ANS was also used to study the aggregation behavior of **1** since it has an intriguing luminescence property.²² Fluorescence of ANS is largely quenched in aqueous media due to the dynamic collisional quenching, whereas in the presence of aggregates (having hydrophobic cavities/clefts), fluorescence intensity increases. Results obtained from ANS-binding studies (under equilibrium conditions) also supported the secondary aggregation model for the gelation of **1** (Figure 4). A small difference in the critical aggregation concentrations determined by pyrene and ANS can be attributed to the fact that ANS may have additional electrostatic interactions with the aggregates, resulting in a change in the emission property when bound to pre-micellar aggregates. In the gel state, the fluorescence intensity of ANS increased severalfold (30-fold for $[\mathbf{1}] = 5.3$ mM in 20% AcOH–water). Figure 1B shows a bright luminescent gel photographed in a dark room by illuminating it with a long-wavelength UV lamp. A blue shift of the emission maxima from 520 to 470 nm in the course of the gelation further supports the change in the local environment of ANS. Both the increase in the intensity and the blue shift of ANS fluorescence were attributed to the trapping of ANS in the hydrophobic pockets created in the gel phase. This hypothesis was further supported by fluorescence anisotropy data of ANS in the gel phase. Steady-state fluores-

cence anisotropy (r_{ss}) is an excellent indicator of flexibility of the (supra) molecular structure to which the probe is bound. This reports the dampening of the rotational motion of the fluorescent dye in the time-scale of fluorescence.²³ Variable temperature fluorescence anisotropy of ANS was measured, and the anisotropy was found to diminish in the temperature range of 40–50 °C (Figure 6). Upon gel melting, the rotational mobility of ANS molecules increases, resulting in the drop in the anisotropy. The variable temperature fluorescence anisotropy of ANS exhibits a more gradual decrease compared to the sharp decrease in the molar ellipticity observed in the variable temperature CD. This is not surprising since these two experiments probe two fundamentally different properties, namely, the supramolecular structure of the gel, which is related to the amplification in the chirality, and the diffusional fluidity of the microstructure of the gel, which is related to fluorescence anisotropy of a bound dye. Also, the hysteresis, with melting and freezing points being distinctly different, is typified by the “gel-to-sol” phase transition, as observed by us earlier for organogels.²⁴

3.4. Insights into the Gelation Process Using a Double-Kinetics Approach. The time-resolved decay of the fluorescence anisotropy of probes carries information on the molecular tumbling in the picosecond to nanosecond time regime. In the steady-state fluorescence measurements, retrieval of information is limited due to the fact that steady-state parameters depend on several molecular properties. Time-resolved fluorescence anisotropy measurements, using a picosecond laser, provide insights into the local and global dynamics of complex molecular systems.²⁵ Since the decay kinetics can be resolved as a sum of exponentials, it is possible to selectively probe different local environments in a *microheterogeneous* system, such as a gel. We have earlier shown that a hydrophobic dye, like DPH, has a single population (evident by a single-exponential fluorescence anisotropy decay kinetics) in the gel phase solubilized in the hydrophobic pockets, whereas a partially water-soluble probe, like ANS, distributes between the aqueous phase and the network of the gel (double exponential).¹⁵ ANS has a faster tumbling (single-exponential decay yielding $\phi \approx 0.1$ ns) in isotropic aqueous solutions of low viscosity. In the presence of smaller aggregates (pre-micellar, below CAC_1) of **1**, ANS shows bi-exponential decay kinetics in the fluorescence anisotropy decay. In the micellar aggregates (above CAC_1 , below MGC; see also Figure 4), longer rotational correlation time (ϕ_b for bound ANS) increases to about 5 ns, which is attributed to the increase in the aggregate size. However, the free aqueous ANS does not show any significant increase in the rotational correlation time ($\phi_f \leq 0.2$ ns) in aggregates or in aqueous solutions. In the gel state (above MGC), both the rotational correlation times of ANS (ϕ_b and ϕ_f) showed marked increase. Therefore, we envisioned that the change in the rotational dynamics of ANS, partitioned in the aqueous phase as a function of time during the gelation (kinetic experiments), would carry the information on the changing interfacial water structure around the gel fiber network during the gelation. The time-resolved anisotropy decay profiles of ANS fluorescence at different times (Table 4) indicate that the dynamics of ANS is progressively slowed during the gelation process. The decay profiles indicate the increase in both long and short rotational correlation times upon gelation (Figure 8, 4 and 126 min after

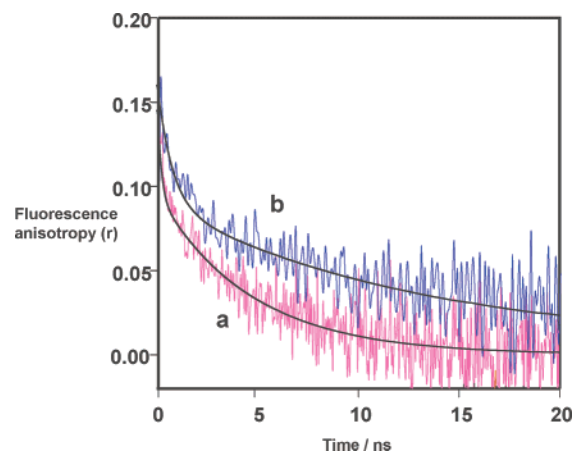


Figure 8. Time-resolved anisotropy decay profiles of ANS at two different times during the gelation of **1** (5.3 mM) in 20% AcOH–water at 25 °C. (a) At 4 min after mixing (pink): $\phi_b = 3.7$ ns, $\phi_f = 0.2$ ns, and $\chi^2 = 1.11$. (b) At 126 min after mixing (blue): $\phi_b = 11.0$ ns, $\phi_f = 1.0$ ns, and $\chi^2 = 1.10$. Solid black lines are the fits.

mixing). According to the Stokes–Einstein equation (eq 2), the change in the rotational correlation time (ϕ) could be explained in terms of the volume of the rotating unit (V) and the microviscosity (η) felt by the probe. Thus, the increase in the longer rotational correlation time (ϕ_b), from 3.7 to 12.1 ns, is ascribed to an increase in both the aggregate size and the microviscosity experienced by the ANS molecules bound to the aggregates of **1**. Our data on the time course of the average translational diffusion of the aggregates (from dynamic light-scattering experiments, Figure 7) also support the present observation on the dynamics of ANS incorporated within the aggregate. The increase in both aggregate size and viscosity would cause the dampening of both translational and rotational dynamics (eqs 1 and 2). The formation of an intertwined network in the gel phase causes the dampening of the tumbling of bound ANS molecules. Additionally, the time-course of the dynamics of free aqueous ANS (characterized by a short rotational correlation time, ϕ_f) seems to be even more interesting. After 4 min of the mixing, ϕ_f was ~ 0.2 ns, which is very close to the value (~ 0.1 ns) obtained for ANS in an aqueous solution of low viscosity (~ 1 cP). With gelation time, ϕ_f becomes progressively longer, which is indicative of incremental change in the microviscosity of the aqueous phase, suggesting the microstructural change caused by the rigidification of the aqueous pool encompassed by the networked nanofibers. We would like to point out that the information about the partial immobilization of solvent molecules (expressed in terms of local viscosity) around the gel network could be experimentally probed by the time-resolved fluorescence. This rigidification is likely to be caused by the entanglement of the long nanofibers (Figure 1) during the gelation process.

3.5. Microviscosity and Bulk Viscosity. In light of our time-resolved fluorescence data, it is necessary to address the issue of microviscosity and bulk viscosity of the gel. The gel derived from **1** (5.3 mM in 20% AcOH–water) does not flow, which means the bulk (macroscopic) viscosity of the gel is much higher (indeterminable using classical techniques) compared to that of glycerol ($\sim 10^3$ cP at 25 °C), which flows. Small molecule fluorescent probes, such as ANS, are expected to show considerably long rotational dynamics (> 100 ns, calculated using eq 2),²⁶ which is not possible to be accessed by the time

window set by the fluorescence lifetime (tens of nanoseconds); as a result, fluorescence anisotropy would show an incomplete depolarization in the time-scale of fluorescence. However, it is interesting to learn that, despite our gels having much higher bulk viscosity, the time-resolved fluorescence anisotropy exhibits complete depolarization with time constants of 12.1 and 1.0 ns. Therefore, we conclude that the microscopic dynamics is much faster compared to that we anticipate by visual observations. For an isotropic medium, such as glycerol, microviscosity experienced by a fluorescent probe is comparable with the bulk viscosity of the fluid. The enormous increase in the bulk viscosity of the gel is thus attributed to the formation of an entangled network comprising of nanofibers. The microviscosity of the aqueous phase around the network of nanofibers is only about 10-fold higher compared to bulk water and far less compared to the bulk viscosity of the gel.

4. Conclusion

We have extensively studied gels obtained from tripodal cholamide **1** in aqueous media using various techniques involving cryo-TEM, CD, steady-state and time-resolved fluorescence, and dynamic light-scattering. Our equilibrium studies shed light into the complex nature of the gel network. A picture of the gel could be constructed as follows. Molecules of **1** aggregate in an asymmetric manner to yield an entangled network structure of nanofibers having a relatively immobilized aqueous compartment. The kinetic data on the gelation addressed the issue related to progressive ordering of the solvent molecules around the network of nanoscale fibers. Our findings concerning the incremental change in both aggregate size and microviscosity of the aqueous pool will be useful for other hydrogel systems. It would be interesting to undertake further studies to understand the structure and dynamics of solvent molecules entrapped in the gel network.

5. Experimental Section

5.1. Syntheses and Characterizations. All of the reactions were carried out in oven-dried round-bottom flasks. TLC was done using precoated TLC plates (0.25 mm silica gel, with fluorescent indicator UV₂₅₄) obtained from Aldrich. After the elution, TLC plates were developed using Libermann–Buehard reagent. For column chromatography, commercial grade solvents were distilled prior to use. Gravity columns were run with silica gel (100–200 mesh) and neutral alumina (~150 mesh, 58 Å) obtained from Aldrich.

Compound 7: Cholic acid **5** (5.21 g, 12.5 mmol) was dissolved in formic acid (19 mL, 0.4 mol), and the mixture was stirred at 55 °C for 5 h. Excess formic acid was removed under reduced pressure, and the free-flowing solid was crystallized from an ethanol–water mixture (50/75 mL). The crystals were washed with an ethanol–water mixture (1:1.5) and dried in a desiccator to yield 5.23 g (83%) of a white solid: mp = 203–204 °C (lit.²⁷ mp 206–207 °C). ¹H NMR (CDCl₃, 300 MHz) δ: 0.762 (s, 3H), 0.852 (d, *J* = 6.6 Hz, 3H), 0.940 (s, 3H), 1.05–1.18 (m, 3H), 1.27–2.43 (m), 4.68–4.73 (m, 1H), 5.071 (br s, 1H), 5.27 (br s, 1H), 8.025 (s, 1H), 8.108 (s, 1H), 8.165 (s, 1H). ¹³C NMR (CDCl₃, 75 MHz) δ: 12.13, 17.42, 22.31, 22.74, 25.51, 26.54, 27.12, 28.52, 30.37, 30.80, 31.30, 34.25, 34.41, 34.49, 34.68, 37.69, 40.76, 42.94, 45.00, 47.18, 70.66, 73.72, 75.25, 160.50, 160.59, 179.79.

Compound 9: To dry CH₂Cl₂ (10 mL), taken in a 50 mL RB flask and cooled in an ice bath, were added triformyl cholic acid **7** (6.7 g, 13.6 mmol), DCC (3.9 g, 18.9 mmol), and DMAP (1.6 g, 13.1 mmol), and the mixture was stirred. After 10 min, tris(2-aminoethyl)amine (400 μL, 2.7 mmol) was added. The reaction was monitored by TLC (6% EtOH–CHCl₃). After 12 h, CHCl₃ (30 mL) was added to the reaction

mixture and filtered through a sintered glass funnel, and the filtrate was washed with water (40 mL), saturated NaHCO₃ (40 mL), and finally with water (40 mL). The organic layer was dried over anhydrous Na₂SO₄ and evaporated to dryness. The crude product was purified by column chromatography (25 cm × 2.6 cm silica column) using 2% EtOH–CHCl₃ to yield 3.6 g (62%) of a colorless product: mp = 179–181 °C. ¹H NMR (CDCl₃, 300 MHz) δ: 0.753 (s, 9H), 0.835 (d, *J* = 6.3 Hz, 9H), 0.954 (s, 9H), 1.09–2.16 (m), 2.53 (m, 3H), 3.25 (m, 6H), 4.72 (m, 3H), 5.075 (s, 3H), 5.268 (s, 3H), 6.434 (t, 3H), 8.027 (s, 3H), 8.111 (s, 3H), 8.169 (s, 3H). ¹³C NMR (CDCl₃, 75 MHz) δ: 12.14, 17.56, 22.31, 22.76, 25.54, 26.54, 27.18, 28.52, 31.30, 31.45, 33.41, 34.25, 34.48, 34.40, 35.00, 37.65, 40.75, 42.92, 45.00, 47.46, 54.61, 70.63, 73.70, 75.22, 77.20, 160.56, 173.92. IR (neat, in cm⁻¹) *ν*: 1716 (s), 1643 (m). MALDI-TOF MS: [M + H]⁺ calcd for C₈₇H₁₃₂N₄O₂₁, 1569.9; found, 1569.5. [α]_D²⁴ +39° (c 1, EtOH).

Compound 1: Compound **5** (750 mg, 0.5 mmol) was dissolved in a 2% KOH/MeOH solution (50 mL), and the mixture was stirred for 14 h at room temperature. Volatiles were removed under reduced pressure, and the residue was dissolved in 25% EtOH/CHCl₃ (10 mL), filtered, and evaporated to dryness. The crude product was purified by column chromatography on neutral alumina (22 × 1.6 cm) with a 5–15% gradient of EtOH in CHCl₃ to yield 355 mg (56%) of a white solid: mp = 192–194 °C. ¹H NMR (DMSO-*d*₆, 300 MHz) δ: 0.558 (s, 9H), 0.792 (s, 9H), 0.904 (d, *J* = 1.2 Hz, 9H), 3.05 (m, 9H), 3.60 (br s, 3H), 3.76 (br s, 3H), 4.00 (m, 3H), 4.09 (m, 3H), 4.39 (m, 3H), 7.70 (t, 3H). ¹H NMR (CDCl₃, 300 MHz) δ: 0.680 (s, 9H), 0.879 (s, 9H), 1.054 (d, *J* = 5.7 Hz, 9H), 1.22–1.55 (m, 18H), 1.75 (br m), 3.75 (m, 3H), 3.82 (m, 3H), 3.96 (m, 3H), 6.91 (m, 3H). ¹³C NMR (DMSO-*d*₆, 75 MHz) δ: 12.36, 17.13, 19.14, 22.61, 22.84, 26.22, 27.30, 28.56, 30.40, 30.48, 31.70, 32.66, 34.40, 34.90, 35.20, 36.93, 41.34, 41.53, 45.76, 46.29, 53.62, 62.79, 66.28, 67.75, 70.45, 71.04, 172.72. IR (Nujol, in cm⁻¹) *ν*: 3338 (m br), 1642 (m), 1549 (w). MALDI-TOF MS: [M + H]⁺ calcd for C₇₈H₁₃₂N₄O₁₂, 1318.0; found, 1318.2. HRMS: calcd 1317.9920; found 1317.9552. Anal. Calcd for C₇₈H₁₃₂N₄O₁₂·5H₂O: C, 66.54; H, 10.16; N, 3.98. Found: C, 66.72; H, 9.77; N, 3.75. [α]_D²⁴ +27° (c 2, EtOH).

Compound 8: Deoxycholic acid **6** (5.18 g, 13 mmol) was dissolved in formic acid (15 mL, 0.39 mol), and the mixture was stirred at 55 °C for 7 h. Excess formic acid was removed under reduced pressure. Then, the free-flowing solid was crystallized from an ethanol–water mixture (44/22 mL) and filtered through a Buchner funnel. Then, it was washed with an ethanol–water mixture (2:1) and dried in a desiccator for 2 days to yield 5.24 g (88%): mp = 189–190 °C. ¹H NMR (CDCl₃, 300 MHz) δ: 0.73 (s, 3H), 0.82 (d, *J* = 6.0 Hz, 3H), 0.90 (s, 3H), 0.97–2.36 (m), 4.81 (m, 1H), 5.23 (br s, 1H), 8.01 (s, 1H), 8.11 (s, 1H).

Compound 10: To dry CH₂Cl₂ (10 mL), taken in an RB flask and cooled in an ice–water bath, were added diformyl deoxycholic acid (5.01 g, 11 mmol), DCC (2.83 g, 13 mmol), and DMAP (1.5 g, 12 mmol), and the mixture was stirred. After 10 min, tris(2-aminoethyl)amine (325 μL, 2.2 mmol) was added. The mixture was stirred at room temperature for 18 h. CHCl₃ (30 mL) was added to the reaction mixture. The mixture was filtered through a sintered funnel, and the filtrate was washed with water (40 mL), saturated aqueous NaHCO₃ (40 mL), and finally with water (40 mL). The solvent was evaporated, and the residue was dried in vacuo. The crude product was purified by column chromatography (20 × 2.5 cm silica column) using 2% EtOH–CHCl₃ to yield 1.60 g (50%) of a colorless product: mp = 142–143 °C. ¹H NMR (CDCl₃, 300 MHz) δ: 0.746 (s, 9H), 0.835 (d, *J* = 6.3 Hz, 9H), 0.928 (s, 9H), 1.26–1.90 (m), 2.53 (br t, 4H), 3.25 (br d, *J* = 4.2 Hz, 6H), 4.80 (m, 3H), 5.25 (br s, 3H), 6.40 (br t, 3H), 8.026 (s, 3H), 8.131 (s, 3H). ¹³C NMR (CDCl₃, 75 MHz) δ: 12.40, 17.56, 22.31, 22.76, 25.54, 26.54, 27.18, 28.52, 31.30, 31.45, 33.41, 34.25, 34.40, 34.48, 35.00, 37.65, 40.75, 42.92, 45.00, 47.46, 54.61, 70.63, 73.70, 75.22, 77.21, 160.56, 160.60, 173.92. IR (neat, in cm⁻¹) *ν*: 1721 (s), 1642 (m). MALDI-TOF MS: [M + H]⁺ calcd for C₈₄H₁₃₂N₄O₁₅, 1438.0; found, 1438.4. [α]_D²⁴ +63° (c 1, EtOH).

Compound 2: Compound **6** (550 mg, 0.4 mmol) was dissolved in a 2% KOH–MeOH solution (50 mL), and the mixture was stirred at room temperature for 14 h. The volatiles were pumped off, and the residue was dissolved in 25% EtOH–CHCl₃ (5 mL), filtered, and evaporated to dryness. The crude product obtained was purified by column chromatography on neutral alumina (22 × 1.6 cm) with 10% EtOH–CHCl₃ to afford 284 mg (56%) of a colorless product: mp = 164–165 °C. ¹H NMR (DMSO-*d*₆, 300 MHz) δ: 0.458 (s, 9H), 0.718 (s, 9H), 0.790 (d, *J* = 5.7 Hz, 9H), 0.938–2.007 (m), 2.35 (br d, 4H), 2.94 (m, 6H), 4.07 (m, 3H), 4.12 (m, 3H), 7.57 (t, 3H). ¹³C NMR (DMSO-*d*₆, 75 MHz) δ: 12.46, 17.10, 23.10, 23.58, 26.18, 27.05, 27.23, 28.64, 30.24, 31.72, 32.64, 32.95, 33.84, 35.17, 35.70, 36.31, 37.00, 41.65, 46.00, 46.31, 47.45, 56.08, 70.00, 71.07, 79.19, 172.78. IR (Nujol, in cm⁻¹) *ν*: 3365 (m), 1644 (m). MALDI-TOF MS: [M + Na]⁺ calcd for C₇₈H₁₃₂N₄O₉, 1292.0; found, 1293.6. HRMS: [M + H]⁺ calcd 1270.0072; found 1270.0249. Anal. Calcd for C₇₈H₁₃₂N₄O₉·4H₂O: C, 69.81; H, 10.51; N, 3.17. Found: C, 70.03; H, 10.36; N, 3.42. [α]_D²⁴ +52° (c 2, C₂H₅OH).

Compound 11: To CH₂Cl₂ (2 mL) were added trimethylcholic acid (550 mg, 1.1 mmol), DCC (290 mg, 1.5 mmol), and DMAP (141 mg, 1.1 mmol) at 0 °C. *N,N*-Dimethylethylenediamine (110 μL, 1.0 mmol) was added to the mixture after 5 min. The mixture was stirred at room temperature for 18 h. The reaction mixture was diluted with 20 mL of CH₂Cl₂. It was filtered, and the filtrate was washed with water (20 mL), saturated aqueous NaHCO₃ (20 mL), and water (20 mL). The organic layer was dried over anhydrous Na₂SO₄; the solvent was evaporated, and the residue was dried in vacuo. Purification of the crude product by column chromatography (12 × 2.5 cm silica column) using 3% EtOH–CHCl₃ yielded 150 mg (45%) of a colorless product: mp = 143–144 °C. ¹H NMR (CDCl₃, 300 MHz) δ: 0.753 (s, 3H), 0.840 (d, *J* = 6.3 Hz, 3H), 0.897 (s, 3H), 0.95–2.27 (m), 2.334 (s, 6H), 2.428 (t, *J* = 6 Hz, 2H), 3.320 (dd, *J*₁ = 5.4 Hz, *J*₂ = 6.0 Hz, 2H), 4.67 (m, 1H), 5.06 (m, 1H), 5.16 (m, 1H), 6.35 (br m, 1H), 8.026 (s, 1H), 8.105 (s, 1H), 8.162 (s, 1H). ¹³C NMR (CDCl₃, 75 MHz) δ: 12.14, 17.46, 17.56, 22.31, 22.76, 25.54, 26.54, 27.18, 28.52, 31.30, 31.45, 33.41, 34.25, 34.40, 34.48, 35.00, 37.65, 40.75, 42.92, 45.00, 47.46, 54.61, 70.63, 73.70, 75.22, 160.56, 173.92. IR (neat, in cm⁻¹) *ν*: 1722 (s), 1643 (m). MALDI-TOF MS: [M + H]⁺ calcd for C₃₁H₅₀N₂O₇, 564.4; found, 564.6. [α]_D²⁴ +45° (c 1, EtOH).

Compound 3: Compound **11** (150 mg, 0.2 mmol) was dissolved in a 2% KOH–MeOH solution (2 mL), and the mixture was stirred for 14 h. The volatiles were removed; the residue was dissolved in 25% EtOH–CHCl₃ (10 mL) and filtered, and the filtrate was evaporated. The crude product was purified by column chromatography on neutral alumina (18 × 2.6 cm) with 10% EtOH–CHCl₃ as eluent to yield 75 mg (60%) of a colorless product: mp = 159–162 °C. ¹H NMR (CDCl₃, 300 MHz) δ: 0.666 (s, 3H), 0.880 (s, 3H), 0.999 (d, *J* = 5.4 Hz, 3H), 1.09–2.17 (m), 2.243 (s, 6H), 2.419 (t, *J* = 6.0 Hz, 2H), 3.310 (dd, *J*₁ = 6.0 Hz, *J*₂ = 6.9 Hz, 2H), 3.71 (m, 1H), 3.82 (m, 1H), 3.94 (m, 1H), 6.61 (br t, 1H). ¹³C NMR (CDCl₃, 75 MHz) δ: 12.46, 17.50, 22.50, 23.32, 26.34, 27.61, 30.53, 31.70, 33.10, 34.76, 34.80, 35.42, 35.50, 36.75, 39.49, 39.64, 41.61, 45.14, 46.36, 46.41, 58.11, 63.72, 68.38, 71.75, 73.02, 77.26, 174.38. IR (Nujol, in cm⁻¹) *ν*: 3347 (m), 1650 (m). MALDI-TOF MS: [M + H]⁺ calcd for C₂₈H₅₀O₄N₂, 479.4; found, 480.8. HRMS: calcd 479.3848; found 479.3821. [α]_D²⁴ +32° (c 1, EtOH).

Compound 12: To dry CH₂Cl₂ (2 mL) were added diformyl deoxycholic acid (1.1 g, 2.4 mmol), DCC (0.6 g, 2.9 mmol), and DMAP (0.4 g, 3.2 mmol) under cold conditions. The mixture was placed in an ice–water bath, and after 5 min, *N,N*-dimethylethylenediamine (220 μL, 2.0 mmol) was added. The mixture was stirred for 16 h. CHCl₃ (30 mL) was added, and the mixture was filtered. The filtrate was washed with water (30 mL), saturated aqueous NaHCO₃ (30 mL), and water (30 mL). The organic layer was dried over anhydrous Na₂SO₄. The solvent was evaporated, and the residue was dried in vacuo.

The crude product was purified by column chromatography (22 × 4.6 cm silica column) using 2% EtOH–CHCl₃ to yield 0.5 g (59%) of a colorless product: mp = 101–103 °C. ¹H NMR (CDCl₃, 300 MHz) δ: 0.745 (s, 3H), 0.837 (d, *J* = 6.3 Hz, 3H), 0.925 (s, 3H), 1.0–2.1 (m), 2.236 (s, 6H), 2.408 (t, *J* = 5.4 Hz, 2H), 3.315 (dd, *J*₁ = 5.4 Hz, *J*₂ = 5.7 Hz, 2H), 4.83 (m, 1H), 5.25 (br s, 1H), 6.01 (br s), 8.028 (s, 1H), 8.131 (s, 1H). ¹³C NMR (CDCl₃, 75 MHz) δ: 12.24, 17.44, 22.80, 23.32, 25.63, 25.78, 26.35, 26.66, 27.24, 31.32, 31.98, 33.24, 33.90, 34.08, 34.56, 34.82, 35.48, 36.53, 41.62, 44.94, 47.36, 49.13, 57.80, 73.97, 75.91, 160.45, 160.53, 173.35. IR (neat, in cm⁻¹) *ν*: 1724 (s), 1643 (m). MALDI-TOF MS: [M + H]⁺ calcd for C₃₀H₅₀N₂O₅, 519.5; found, 519.8. [α]_D²⁴ +62° (c 1, EtOH).

Compound 4: Compound **12** (150 mg, 0.2 mmol) was dissolved in a 2% KOH–MeOH solution (2 mL), and the mixture was stirred for 14 h. The volatiles were removed; the residue was dissolved in 25% EtOH–CHCl₃ (10 mL) and filtered, and the filtrate was evaporated. The crude product was purified by column chromatography on neutral alumina (18 × 2.6 cm) with 10% EtOH–CHCl₃ as eluent to yield 75 mg (60%) of a colorless product: mp = 114–115 °C. ¹H NMR (CDCl₃, 300 MHz) δ: 0.677 (s, 3H), 0.907 (s, 3H), 0.970 (d, *J* = 6.0 Hz, 3H), 1.0–1.8 (m), 2.236 (s, 6H), 2.414 (t, *J* = 5.1 Hz, 2H), 3.33 (m, 2H), 3.60 (m, 3H), 3.97 (br s, 3H), 6.55 (br m). ¹³C NMR (CDCl₃, 75 MHz) δ: 12.69, 17.39, 23.10, 23.68, 26.13, 27.12, 27.48, 28.59, 30.40, 31.63, 33.31, 33.56, 34.09, 35.22, 35.29, 35.95, 36.42, 36.53, 42.03, 45.00, 46.45, 46.77, 48.14, 58.00, 71.53, 72.99, 174.99. IR (Nujol, cm⁻¹) *ν*: 3328 (m), 1652 (m). MALDI-TOF MS: [M + H]⁺ calcd for C₂₈H₅₀N₂O₃, 463.4; found, 463.8. HRMS: calcd 463.3899; found 463.3902. [α]_D²⁴ +35° (c 1, EtOH).

5.2. Test of Gelation and Measurements of *T*_{gel}. Gelation tests were performed in 5 mm diameter Pyrex test tubes. The inverted tube method was adopted to measure the *T*_{gel} of the samples.²⁸ For all *T*_{gel} measurements, 5 mm diameter sealed test tubes with 0.5 mL of solvents were used.

5.3. Cryo-TEM. We prepared cryogenic temperature transmission electron microscopy (cryo-TEM) specimens in a controlled-environment vitrification system (CEVS), as previously described.^{29a} Specimens were quenched from 25 °C and 100% relative humidity to prevent solvent loss during specimen preparation. We imaged the vitrified specimens in a Philips CM120 cryo-dedicated TEM, equipped with an Oxford CT3500 cryo-holder system to maintain the specimens in the TEM at about –180 °C. The TEM was operated with an acceleration voltage of 120 kV. Images were recorded digitally with a Gatan MultiScan 791 cool-CCD camera system.

5.4. Circular Dichroism. Variable temperature CD spectra were recorded using a JASCO J715 spectropolarimeter, equipped with a Peltier temperature controller (JASCO PTC-348W1). All of the samples were filtered through a 0.45 μm filter into a 0.5 mm path length quartz cuvette and were allowed to form a gel. For variable temperature CD experiments, samples were equilibrated for 10 min at every temperature at which measurements were carried out.

5.5. Steady-State Fluorescence. Steady-state fluorescence spectra were recorded on a Perkin-Elmer luminescence spectrometer (LS-50B). ANS was obtained from Fluka (>98%) and was used without further purification. ANS stock solution (1 mM) was prepared in double distilled water, which was diluted to a final concentration of 10 μM for all of the experiments. Samples were excited at 365 nm, and emissions were measured at 475 nm. For fluorescence anisotropy (eq 6) measurements, perpendicular components of the emitted light (*I*_⊥) were corrected with respect to the *G* factor of the instrument. A water circulator (Julabo F25) connected to the sample accessory using thermally insulating tubes was used for controlling the temperature. For variable temperature anisotropy experiments, samples were equilibrated for 10 min at every temperature at which measurements were carried out.

$$r = \frac{I_{\parallel} - GI_{\perp}}{I_{\parallel} + 2GI_{\perp}} \quad (6)$$

Pyrene was obtained from Aldrich and was purified on a silica column using petroleum ether followed by a recrystallization from methanol. A saturated solution of pyrene was prepared in water by sonication for 2 h followed by filtration. The concentration of pyrene in saturated solution was found to be 0.5 μM (UV method). Samples were excited at 337 nm. I_1 and I_3 were measured at 373 and 384 nm, respectively. Excimer intensities were measured at 475 nm.

5.6. Fluorescence Lifetime Measurements. Time-resolved fluorescence decays were measured using a N_2 flash lamp of short duration, equipped with a time-correlated single photon counting (TCSPC) obtained from IBH. Full width at half-maxima (fwhm) of the pulse was ~ 1.1 ns. All data were deconvoluted with respect to the lamp profile and analyzed using IBH software that was provided with the instrument. Data were fitted using single- or multiexponential fits using the nonlinear least-squares method. Fluorescence lifetime of pyrene in deoxygenated water was 174 ± 5 ns (reported previously as 175 ns).³⁰ Pyrene solution was deoxygenated using three cycles of freeze–pump–thaw. For micelle and gel samples, pyrene solution was used without deoxygenation.

5.7. Dynamic Light-Scattering Experiments. Dynamic light-scattering experiments were performed on a DynaPro-MS800 instrument (Protein Solution Inc., VA), which monitors the scattered light at 90° . Acetic acid and water were filtered through 0.02 μm filters followed by centrifugation at 12 000 rpm for 20 min before adding the mixture to the gelator. “Regularization” software, provided with the instrument, was used to analyze the data to obtain the hydrodynamic radius. A solution of bovine serum albumin (3 nm) was used as a standard.

5.8. Time-Resolved Fluorescence Anisotropy Measurements. Time-resolved fluorescence decay measurements of the samples were made using a high repetition-rate picosecond laser (frequency-tripled Ti–Sapphire laser) coupled to a time-correlated single photon counting (TCSPC) setup. A Ti–Sapphire femto/picosecond laser (Spectra Physics, Mountain View, CA) pumped by an Nd:YLF laser (Millenia X, Spectra Physics) was used. Pulses of 1 ps duration of 921 nm radiation from the Ti–Sapphire laser were frequency tripled to 307 nm by using a frequency doubler/tripler (GWU, Spectra Physics). Fluorescence decay curves were obtained by using the TCSPC setup, coupled to a microchannel plate photomultiplier (Model 2809u, Hamamatsu Corp.). The instrument response function (IRF) was obtained at 307 nm using a dilute colloidal suspension of dried nondairy coffee whitener. The width (fwhm) of the IRF was ~ 40 ps. The samples

were excited at 307 nm, and emissions were measured at 490 nm. For all of the measurements, 10K counts were collected. For time-resolved anisotropy measurements, the emission data were collected at 0 and 90° with respect to the excitation polarization, and the time-resolved anisotropy decays were analyzed by globally fitting $I_{\parallel}(t)$ and $I_{\perp}(t)$:

$$I_{\parallel}(t) = I(t)[1 + 2r(t)]/3 \quad (7)$$

$$I_{\perp}(t) = I(t)[1 - r(t)]/3 \quad (8)$$

The perpendicular component of the fluorescence decay was corrected for the G factor of the spectrometer. $I(t)$ is the fluorescence intensity collected at the magic angle (54.7°) at time t . The anisotropy decays were analyzed according to the two-population model, wherein ANS was assumed to be distributed between two phases (free and bound). The time-dependent anisotropy $r(t)$ is represented by eq 9.³¹

$$r(t) = f_f(t)r_f(t) + f_b(t)r_b(t) \quad (9)$$

where $f_f(t)$ and $f_b(t)$ are the fractions of the emitted photons corresponding to the free and bound ANS at time t , respectively; $r_f(t)$ and $r_b(t)$ are the anisotropy decay functions of the free and bound ANS, respectively.

$$r_f(t) = r_{0f} \exp(-t/\phi_f) \quad (10)$$

$$r_b(t) = r_{0b} \exp(-t/\phi_b) \quad (11)$$

where r_{0f} and r_{0b} are the initial anisotropies, and ϕ_f and ϕ_b are the rotational correlation times of ANS in two phases (free and bound, respectively).

The intensity fraction, $f_f(t)$, is given by

$$f_f(t) = [x_f[\alpha_{f1} \exp(-t/\tau_{f1}) + \alpha_{f2} \exp(-t/\tau_{f2})]] / [x_f[\alpha_{f1} \exp(-t/\tau_{f1}) + \alpha_{f2} \exp(-t/\tau_{f2})] + x_b[\alpha_{b1} \exp(-t/\tau_{b1}) + \alpha_{b2} \exp(-t/\tau_{b2})]] \quad (12)$$

where x_f and x_b are the fractions of free and bound probes, respectively. τ_{f1} and τ_{f2} are the fluorescence lifetimes of free ANS, and τ_{b1} and τ_{b2} are the fluorescence lifetimes of bound ANS. The free and bound ANS had two fluorescence lifetimes.

Acknowledgment. We thank the Jawaharlal Nehru Centre for Advanced Scientific Research (Bangalore) for financial support, and Professor N. Periasamy (TIFR, Mumbai) for providing us the software for the fluorescence decay analysis. We also thank Professor P. K. Das (IISc, Bangalore) for helping us with fluorescence lifetime measurements.

JA046788T

(30) Vethamathu, M. S.; Almgren, M.; Mukhtar, E.; Bahadur, P. *Langmuir* **1992**, *8*, 2396.

(31) (a) Ludescher, R. D.; Peting, L.; Hudson, S.; Hudson, B. *Biophys. Chem.* **1987**, *28*, 59. (b) Srivastava, A.; Krishnamoorthy, G. *Arch. Biochem. Biophys.* **1997**, *340*, 159.